AIAA JOURNAL
Vol. 31, No. 7, July 1993

Spectral Solution of the Viscous Blunt-Body Problem

David A. Kopriva*
Florida State University, Tallahassee, Florida 32306

The viscous blunt-body problem is solved with a shock-fitted Chebyshev spectral method. No explicit artificial viscosity or filtering is needed to obtain smooth, converged solutions. The method is applied to two problems. First, results for the flow over a right circular cylinder in the Mach number range of 5.5–6.0 are compared with experimental data. Second, a solution for a Mach 25 flow over a hyperbolic cone is compared with a viscous shock-layer calculation.

Introduction

SHOCK-FITTED spectral methods have been shown to solve accurately and efficiently the inviscid blunt-body problem.[1-3] The desirable features of the methods are derived from the high-order global interpolation approximations that define the dependent variables.[4] For smooth enough solutions, the error decays exponentially fast. This means that, for a given number of grid points, the solutions are more accurate than a typical finite difference calculation. Reversing this, fewer grid points are required to obtain the same accuracy. High-order interpolations also mean that derivatives of the solution can be calculated accurately.

Applications of spectral methods to the solution of the boundary-layer equations indicate higher order accuracy should be an advantage for the viscous problem as well. Streett et al.[5] compared the accuracy of a Chebyshev and Legendre spectral method with a fourth-order box scheme for the incompressible boundary-layer equations. They found that, for three digit accuracy, the three methods required roughly the same number of grid points. The Chebyshev method required 20 points, whereas the box scheme required 17. However, for 8 digits, the spectral method required 40 points, whereas the fourth-order method required 255. Similar results have been observed for the compressible boundary-layer equations. Pruett and Streett[6] compared a Chebyshev algorithm with a second-order finite difference method. To compute the wall temperature for an adiabatic wall, they found that 77 points were required for the spectral method to obtain the same 5 digit accuracy for which the finite difference method required 400.

To date, there are few applications of spectral methods to the full compressible Navier-Stokes equations in other than periodic geometries. To our knowledge, only Yasuhara et al.[7] have computed the blunt-body problem. They did not show convergence of their solutions, and their calculations required the use of a spatial filter.

In this paper, we describe a shock-fitted Chebyshev spectral method to compute viscous hypersonic flows over blunt cones and wedges. Our purpose is to demonstrate that it is not necessary to add explicit artificial viscosity or to filter to obtain smooth, converged steady-state solutions. Such smoothing is undesirable for three reasons. The overall accuracy is decreased, high-frequency information is eliminated, and artificial viscous effects can be introduced. In the absence of shocks or other discontinuities in the computed region, the need for explicit filtering of smooth solutions often indicates the use of poor boundary procedures that introduce high-frequency errors into the solution. These errors destroy both the accuracy and the convergence rate in steady-state problems.

Shock fitting is used here to insure that differentiation across the shock is not required at high Mach numbers. This avoids the need for any smoothing of the solution to eliminate the Gibbs phenomenon.[4] It also limits the range of applicability of the method to problems where the shock is sharp and can be considered a discontinuity. Moretti and Salas[8] present graphs that show how this range depends on the Mach and Reynolds numbers. The problems considered here, with Mach numbers larger than 5 and Reynolds numbers larger than 2×10^3, fall within the range of applicability of a sharp shock. For very low Reynolds numbers, it should be possible to capture the shock by resolving its structure, but we do not consider this case here.

We apply the method to two problems. We first consider the flow over a right circular cylinder for which experimental results are available in the Mach number range of 5.5–6.0.[9] A heat transfer profile is also compared with a finite difference computation of Gnoffo.[10] The second problem is that of a Mach 25 flow over a cold, isothermal, hyperbolic cone. Detailed comparisons are made with the results of a finite difference viscous shock-layer solution.

Viscous Blunt-Body Problem

We consider the viscous supersonic flow about a blunt-nose wedge or cone at zero angle of attack, as pictured in Fig. 1. Because the flow is symmetric about the centerline of the body, we need to solve only the upper half of the full-flow problem. By fitting the shock as a boundary to the flow, we need only consider the flow in the shock layer, i.e., the region between the shock and the body.

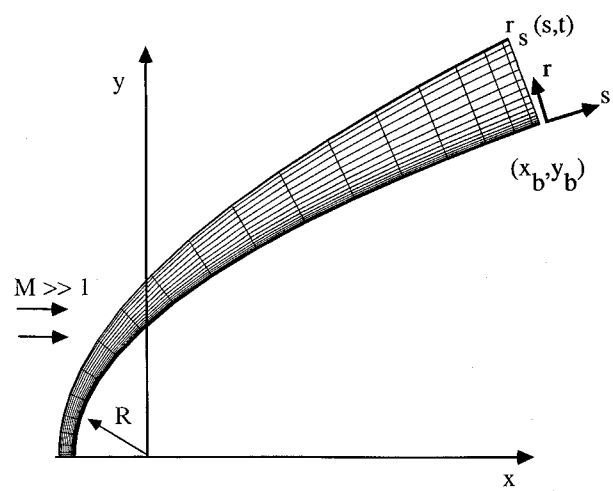

Fig. 1 Diagram of the blunt-body geometry. Computational region uses a stretched Chebyshev grid in the body normal direction.

Received May 1, 1992; revision received Nov. 25, 1992; accepted for publication Dec. 2, 1992.

*Associate Professor, Department of Mathematics and Supercomputer Computations Research Institute. Member AIAA.

Within the shock layer, we solve the Navier-Stokes equations. Following Moretti and Salas,[8] we scale the dimensional pressure, density, velocity, and temperature (p^*, ρ^*, q^*, and T^*) by

$$\begin{aligned} p &= p^*/p_\infty \\ \rho &= \rho^*/\rho_\infty \\ q &= q^*/\sqrt{p_\infty/\rho_\infty} \\ T &= T^*\Big/\left(\frac{p_\infty}{\Re\rho_\infty}\right) \end{aligned} \tag{1a}$$

where $\Re$ is the gas constant. We scale the dimensional space and time by

$$\begin{aligned} x &= x^*/R \\ t &= t^*\sqrt{p_\infty/\rho_\infty}/R \end{aligned} \tag{1b}$$

where R represents the radius of curvature of the body at the nose. Under this scaling, the Navier-Stokes equations become

$$\begin{aligned} &\rho_t + u\rho_x + v\rho_y + \rho u_x + \rho v_y + \frac{\xi\rho v}{y} = 0 \\ &u_t + uu_x + vu_y + \frac{p_x}{\rho} = \frac{\sqrt{\gamma}M_\infty}{\rho Re}\tau^x \\ &v_t + uv_x + vv_y + \frac{p_y}{\rho} = \frac{\sqrt{\gamma}M_\infty}{\rho Re}\tau^y \\ &p_t + up_x + vp_y + \gamma p\,\nabla\cdot q = \frac{\gamma\sqrt{\gamma}M_\infty}{PrRe}\nabla\cdot(\kappa\nabla T) + \frac{(\gamma-1)\sqrt{\gamma}M_\infty}{Re}\Phi \end{aligned} \tag{2}$$

where

$$\begin{aligned} \tau^x &= \frac{\partial}{\partial x}\left[\mu(4u_x - 2v_y)/3 - \frac{2\xi\mu v}{3y}\right] + \frac{\partial}{\partial y}\left[\mu(v_x - u_y)\right] \\ &\quad + \frac{\xi\mu}{y}(v_x + u_y) \\ \tau^y &= \frac{\partial}{\partial x}\left[\mu(v_x + u_y)\right] + \frac{\partial}{\partial y}\left[\mu(4v_y - 2u_x)/3 - \frac{2\xi\mu v}{3y}\right] \\ &\quad + \frac{2\xi\mu}{y}\left(v_y - \frac{v}{y}\right) \\ \Phi &= \frac{\mu u_x}{3}(4u_x - 2v_y) + \mu(u_y + v_x)^2 + \frac{\mu v_y}{3}(4v_y - 2u_x) \\ &\quad + \frac{4\mu\xi}{3}\left[\left(\frac{v}{y}\right)^2 - \frac{v}{y}(u_x + v_y)\right] \end{aligned} \tag{3}$$

The parameter $\xi = 1$ for the axisymmetric case and 0 for two-dimensional flow. We are most interested here in testing the numerical method, and so we consider only an ideal gas equation of state, which becomes

$$T = p/\rho \tag{4}$$

under the scaling of Eq. (1). The sound speed is $a = \sqrt{\gamma T}$. The dimensionless variables in Eqs. (2) are the standard Reynolds number *Re*, which is scaled to the nose radius, the Prandtl number *Pr*, and the Mach number *M*.

To compute the viscosity coefficients, we use the Sutherland law[11]

$$\mu = \frac{\mu^*}{\mu_\infty} = \frac{1 + 198.6/T_r}{T + 198.6/T_r}\,T^{3/2} \tag{5}$$

where $T_r^* = (p_\infty/\Re\rho_\infty) = T_\infty$ is measured in °R. We assume constant Prandtl number, and so the same formula is used to compute κ, the dimensionless coefficient of thermal conductivity.

For axisymmetric problems, there is a coordinate singularity in Eqs. (2) and (3) at the symmetry axis, $y = 0$. To remove the singularity, we use L'Hopital's rule and make the following replacements in the equations at $y = 0$:

$$\begin{aligned} \kappa\frac{T_y}{y} &\to \kappa T_{yy} \\ \frac{v}{y} &\to v_y \\ \frac{v_x}{y} &\to v_{xy} \\ \frac{u_y}{y} &\to u_{yy} \\ \frac{2\mu}{y}\left(v_y - \frac{v}{y}\right) &\to \mu v_{yy} \end{aligned} \tag{6}$$

Spectral Approximation

Mappings and Interior Approximation

Like the inviscid calculation,[2,3] the computational region in Fig. 1 is mapped to a square in two steps: $(x, y, t) \leftrightarrow (r, s, t) \leftrightarrow (X, Y, \tau)$. The first mapping is to a coordinate system where s represents the distance along the body (with $s = 0$ at the nose) and r is the normal distance from the body surface. The mapping $(x, y) \leftrightarrow (r, s)$ is made by the relations

$$\begin{aligned} x &= x_b(s) + r\hat{r}\cdot\hat{x} \\ y &= y_b(s) + r\hat{r}\cdot\hat{y} \end{aligned}$$

where x_b and y_b represent the body as a function of s. Given the shock position $r_{sh}(s, t)$ and an outflow plane $s = s_{max}$, we map the (r, s) space to the unit square $(X, Y) \in [0, 1] \times [0, 1]$ by

$$\begin{aligned} X' &= \frac{r}{r_{sh}(s, t)} \\ Y &= \frac{s}{s_{max}} \end{aligned}$$

To resolve better the boundary layer, a hyperbolic tangent[5] stretching is used in the body-normal direction:

$$X' = \frac{[1 - \tanh(\sigma)]X}{1 - \tanh(\sigma X)} \qquad 0 \le X \le 1$$

When the parameter $\sigma = 0$, there is no stretching.

The interior points are computed with a standard Chebyshev collocation method.[4] A grid is placed on the mapped computational space distributed according to the nodes of the Gauss-Lobatto quadrature rule,

$$\begin{aligned} X_i &= \frac{1}{2}\left[1 - \cos\left(\frac{i\pi}{N}\right)\right] \qquad i = 0, 1, \ldots, N \\ Y_j &= \frac{1}{2}\left[1 - \cos\left(\frac{j\pi}{M}\right)\right] \qquad j = 0, 1, \ldots, M \end{aligned} \tag{7}$$

The primitive variables p, u, v, and ρ are each represented by a Chebyshev polynomial of the form

$$\begin{bmatrix} p \\ u \\ v \\ \rho \end{bmatrix} = U = \sum_{n=0}^{N}\sum_{m=0}^{M} a_{nm}T_n(2X - 1)T_m(2Y - 1) \tag{8}$$

that interpolates globally the values of the solution unknowns at the grid (or collocation) points (X_i, Y_j).

To approximate Eqs. (2) and (3), the derivatives are replaced by the analytical derivatives of Eq. (8) evaluated at the collocation points. For example,

$$\left(\frac{\partial U}{\partial X}\right)_{i,j} = \sum_{n=0}^{N}\sum_{m=0}^{M} a_{nm} T_n'(2X_i - 1) T_m(2Y_j - 1) \tag{9}$$

Equivalently, the differentiation process can be written as a matrix multiplication,

$$\left(\frac{\partial U}{\partial X}\right)_{i,j} = \sum_{k=0}^{N} d_{ik}^X U_{k,j} \tag{10}$$

where D^X is the $(N+1)\times(N+1)$ differentiation matrix for the X direction (see Ref. 4). We use matrix multiplication to compute the derivatives since it is faster and more flexible for the grid sizes used here. Note that, unlike finite difference methods, especially most higher order ones, the spectral method defines derivatives even at the boundaries of the grid.

The result of the spatial discretization is a system of ordinary differential equations for the solution values at the grid points. The midpoint rule is used for the time discretization. No explicit artificial viscosity or spatial filtering is applied either as part of the solution procedure or as a postprocessing procedure.

It is interesting to compare the work required for the viscous spectral code with that required by the inviscid one. Table 1 compares the number of matrix derivatives required for the inviscid and the viscous problems. The derivative calculations typically represent a major portion of the computational cost of a spectral method. Thus, Table 1 indicates the relative amount of work required by the two flow types.

The axisymmetric case requires more derivatives than the two-dimensional case. It is necessary to do global derivative calculations to compute the extra derivative terms in Eq. (6) that arise from the removal of the singularity at the symmetry line. Fortunately, that extra work is not significant. If the number of collocation points in the X and Y directions are N and M, $\mathcal{O}(MN^2)$ multiplications and $\mathcal{O}(NM^2)$ multiplications are required to compute everywhere an X and a Y derivative value. However, the extra derivatives introduced along the symmetry line need only be computed at the symmetry line itself. Thus, only $\mathcal{O}(MN)$ multiplications are required by the additional terms.

Boundary Conditions

The flow equations require both Dirichlet and Neumann type boundary conditions. For spectral collocation methods, Dirichlet conditions are usually imposed in the same manner as they are imposed in a finite difference method. That is, the solution values at the boundary points are replaced by the value of the boundary condition.

Neumann conditions can be applied in one of three ways.[12,13] The first method imposes the condition on the solution directly, or explicitly, using Eq. (10). The second imposes the condition indirectly, or implicitly, when computing second derivative terms. The third method[13] enforces the boundary condition by a penalty term. In the calculations done here, we considered the first two methods.

As an example of the direct method, consider the imposition of the boundary condition

$$\frac{\partial w}{\partial X} = f \tag{11}$$

Table 1 Number of matrix derivatives required for different approximations

Case	No. of matrix derivatives
Inviscid	8
Viscous	20

at the right boundary. Let $\{w_j\}_{j=0}^N$ represent a computed solution at the collocation points $\{X_j\}_{j=0}^N$. The boundary condition is imposed by choosing the last solution point value w_N so that the Chebyshev derivative at the boundary satisfies

$$(\boldsymbol{D}^X \boldsymbol{w})_N = \sum_{k=0}^{N} d_{N,k}^X w_k = f$$

Thus, the direct method gives

$$w_N = \frac{1}{d_{N,N}^X}\left(f - \sum_{k=0}^{N-1} d_{N,k}^X w_k\right) \tag{12}$$

Note that the procedure just described is a spectrally accurate extrapolation of w to the boundary, with the constraint that the spectral derivative at the boundary equals f.

A Neumann condition can also be imposed indirectly when the second derivative terms are calculated. For example, the calculation of a term of the form $(\nu w_x)_x$ subject to the condition that $w_x = 0$ at the right boundary is implemented indirectly by first computing the vector $\boldsymbol{z} = \boldsymbol{D}^X \boldsymbol{w}$. A new vector $\tilde{\boldsymbol{z}}$ is constructed by replacing the last element of $\boldsymbol{z}$ by the boundary condition $z_N = f$. Finally, the result $\boldsymbol{D}^X(\nu\tilde{\boldsymbol{z}})$ is computed. This method does not impose the boundary condition exactly. Rather, the condition (11) is approached spectrally fast as N is increased.[12]

The physical boundary conditions applied at the body surface are

$$u = v = 0$$

$$\begin{cases} T = T_b & \text{(isothermal case)} \\ \dfrac{\partial T}{\partial N} = 0 & \text{(adiabatic case)} \end{cases}$$

Given these conditions, it is still necessary to evaluate the pressure and the density. Spectral methods are well known to be sensitive to the implementation of boundary conditions.[4] This means one must be careful when deriving auxiliary equations to determine the remaining flow variables. It is necessary to insure that the auxiliary conditions are consistent with the global, polynomial nature of the solutions.

To derive the auxiliary conditions, we have made the same observation as that made by Poinsot and Lele.[14] That is, at least for high enough Reynolds numbers, the Navier-Stokes equations propagate waves. This observation allows us to use characteristic ideas to derive the auxiliary conditions on the pressure and density. In matrix form, the system (2) can be written as

$$\boldsymbol{U}_t + \boldsymbol{A}\boldsymbol{U}_\xi + \boldsymbol{B}\boldsymbol{U}_\eta = \boldsymbol{V}(\boldsymbol{U}) \tag{13}$$

where $\boldsymbol{V}(\boldsymbol{U})$ represents the viscous terms and ξ and η represent some locally defined coordinates. Waves propagating, for example, in the ξ direction satisfy

$$\boldsymbol{Z}^{-1}\boldsymbol{U}_t + \Lambda\boldsymbol{Z}^{-1}\boldsymbol{U}_\xi = \boldsymbol{Z}^{-1}[\boldsymbol{V}(\boldsymbol{U}) - \boldsymbol{B}\boldsymbol{U}_\eta] \tag{14}$$

where $\boldsymbol{Z}$ is the matrix of right eigenvectors of $\boldsymbol{A}$, and Λ is the real diagonal matrix of its eigenvalues. At a boundary, say, $\eta = \text{const}$, we select equations from Eq. (14) according to the sign of the entries of Λ, just as in an inviscid flow. Dirichlet conditions are imposed directly. Neumann conditions required by the viscous terms are imposed indirectly as described earlier. Our approach differs from the method of Ref. 14 only in that the full viscous equations are used here to impose the Dirichlet conditions.

To compute the wall pressure, for example, Eq. (14) produces a compatibility equation that relates the pressure and the normal velocity along the inviscid characteristic direction. Let $\hat{N} = (N_1, N_2)$ be the body normal and, for ease of exposi-

tion, define the quantities R_p, R_u, and R_v so that the pressure and momentum equations of Eqs. (2) are written in the form

$$p_t + R_p = 0$$

$$u_t + R_u = 0$$

$$v_t + R_v = 0$$

For the adiabatic case, we impose the temperature boundary condition indirectly in the thermal diffusion terms in the pressure equation. Then Eq. (14), the compatibility equation between the pressure and the normal momentum at the body, is

$$p_t + R_p - \rho a[N_1(u_t + R_u) + N_2(v_t + R_v)] = 0 \tag{15}$$

Application of the no-slip boundary condition yields an equation for the pressure

$$p_t + R_p - \rho a\{N_1 R_u + N_2 R_v\} = 0 \tag{16}$$

that is mapped, discretized, and integrated in the same manner as are the interior point equations.

The density at the body surface is computed from the pressure depending on whether the surface is isothermal or adiabatic. For an isothermal wall, the density is calculated directly from the pressure by the equation of state, Eq. (4). For the adiabatic case we considered two methods. We have found that to compute the density at the wall directly from the continuity equation and computing the pressure from the equation of state is unstable.

The first method for the adiabatic surface condition computes the density so that the density at the wall explicitly satisfies the thermal boundary condition. The adiabatic condition gives a relationship between the normal derivatives of the pressure and the density,

$$\frac{\partial \rho}{\partial N} = \frac{\rho}{p}\frac{\partial p}{\partial N} \tag{17}$$

Once the pressure is computed by the compatibility condition (16), its normal derivative can be computed. The wall density is then computed as in Eq. (12) so that the Eq. (17) is satisfied. To be specific, consider a one-dimensional problem with M collocation points and no mappings. The density derivative at a wall on the left is set to

$$\sum_{m=0}^{M} d_{0,m}\rho_m = \rho_0\left(\frac{1}{p}\frac{\partial p}{\partial N}\right)_{\text{body}} \tag{18}$$

where ρ_0 is the value at the boundary. Equation (18) is a linear equation in ρ_m from which ρ_0 can be found,

$$\rho_0 = \frac{\sum_{m=0}^{M} d_{0,m}\rho_m}{[(1/p)(\partial p/\partial N)]_{\text{body}} - d_{0,0}} \tag{19}$$

The second method for computing the density at an adiabatic surface is to use the appropriate equation from the diagonalized system (14). In this way, the temperature flux condition is imposed implicitly. Specifically, we integrate

$$\rho_t = \frac{1}{a^2}(p_t - V_p) \tag{20}$$

where V_p represents the viscous terms in the pressure equation and p_t is computed by Eq. (16).

The shock boundary is treated as a discontinuity by shock fitting. The procedure is described in detail in Refs. 1 and 2. The only difference is that the compatibility equation (14) that relates the pressure and the normal velocity on the high-pressure (downstream) side of the shock includes the viscous terms in the equations. However, the sharp shock assumption assumes that the viscous terms are negligible near the shock, and so we ignore them.

The outflow boundary is supersonic flow except in the small subsonic portion of the boundary layer near the body surface. Viscous outflow boundary conditions have been considered many times in the literature, for example, in Refs. 15–17. At both the supersonic and subsonic portions of the outflow boundary, we avoid a strong boundary layer by requiring that the normal derivatives of the velocity and temperature vanish. These conditions, along the supersonic parts of the boundary, lead to a well-posed problem.[15] The conditions are imposed indirectly as described earlier.

In the subsonic portion of the boundary layer, one more boundary condition must be specified.[15] For the calculations presented here, we specify the pressure to be a fixed value and typically use the inviscid pressure. It can be obtained either from a Newtonian flow assumption, which is reasonably accurate for hypersonic flows, or from the solution of the inviscid equations. In the comparison later with the viscous shock-layer solutions, the approximate viscous pressure from the finite difference calculation is used. For that calculation, it made little difference which was used, except near the last two or three outflow points.

At subsonic outflow points, we use a streamwise compatibility condition, as represented in Eq. (14), to determine the normal velocity. Let $\hat{N} = (N_1, N_2)$ now be the direction normal to the outflow boundary. Then the compatibility condition between the pressure and the velocity for the normal direction is

$$p_t + R_p + \rho a[N_1(u_t + R_u) + N_2(v_t + R_v)] = 0 \tag{21}$$

The momentum in the direction tangential to the boundary

$$-N_2(u_t + R_u) + N_1(v_t + R_v) \tag{22}$$

is computed from the interior. With p specified and constant in time, $p_t = 0$, the two equations, Eqs. (21) and (22), lead to the outflow equations

$$\begin{aligned} u_t &= -(R_u + N_1 R_p/\rho a) \\ v_t &= -(R_v + N_2 R_p/\rho a) \end{aligned} \tag{23}$$

that are also discretized and integrated in the same manner as are the interior points. For the density, Eq. (14) yields

$$\rho_t = -\left[\frac{1}{a^2}V_p + (\boldsymbol{q}\cdot\hat{N})\hat{N}\cdot\left(\nabla\rho - \frac{1}{a^2}\nabla p\right)\right] \tag{24}$$

Initial Condition

The viscous flow calculation is started from an inviscid solution[1] that is less expensive to compute than the viscous flow. It is from this solution that the outflow pressure is obtained. For the isothermal wall cases, the wall temperature can be significantly different from the temperature at the edge of the thermal boundary layer. In those cases a smooth boundary-layer variation in the velocity and temperature is specified as an initial viscous solution.

Results

To demonstrate the method, we consider two flow problems. The first is the hypersonic flow over a circular cylinder. The computed body surface results for three such flows are compared with experimental results of Tewfik and Giedt.[9] The heat transfer profile for one of the flows is also compared with a finite difference computation of Gnoffo.[10] Finally, we present results of a Mach 25 flow over a 5-deg hyperbolic cone and compare them with a time-dependent shock-fitted finite difference viscous shock-layer[18] (VSL) computation provided by Kumar.[19]

Flow over a Circular Cylinder

To compare the spectral solutions with experiments, three flows over a right circular cylinder of radius $R = 0.242$ in. were computed and compared with the data of Tewfik and Giedt.[9] Table 2 shows the cases run. The Prandtl number for these cases was chosen to be $Pr = 0.77$, which is estimated from the tabular data presented by Hilsenrath et al.[20]

The shock thickness can be estimated from the formula derived by Moretti and Salas[8]:

$$\Delta \approx \frac{8}{3Re}\frac{\gamma}{\gamma+1}\frac{M^2-1}{1+\gamma M^2-\sqrt{2(\gamma+1)M\sqrt{1+[(\gamma-1)/2]M^2}}} \tag{25}$$

According to this formula, the estimated shock thickness is less than 2×10^{-3} in cases I and II and 1×10^{-3} in case III.

Computed results are shown for a 20×15 grid with stretching parameter $\sigma = 0.75$. On this grid, the boundary and thermal layers were approximated near the outflow plane with approximately eight grid points. The time step required on this grid was one-fifth of the inviscid limit. At the shock along the symmetry line, the grid spacing is 7×10^{-3}, so that the estimated shock thickness is small compared with the grid spacing. The calculations were done for θ in the range 0–90 deg, where θ is the polar angle measured from the forward stagnation point. Tewfik and Giedt[9] estimate that the flow separates for θ between 120 and 160 deg in their experiments, and so our calculations terminate well before the separation angle.

The solutions of all of the problems run were smooth and converged to machine precision. In no case was it necessary to add artificial viscosity or to filter the solutions. Figure 2 shows the grid for all three cases and contours of the computed

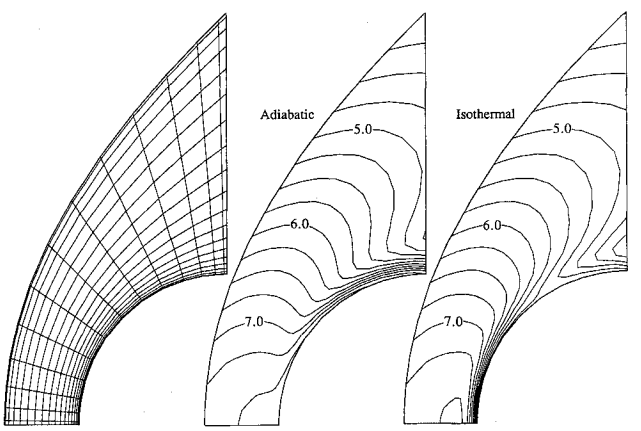

Fig. 2 Grid and temperature contours for flow over a circular cylinder, cases I and II of Table 2.

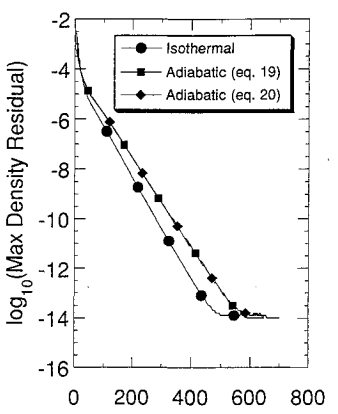

Fig. 3 Convergence of the density for cases I and II of Table 2.

Table 2 Physical parameters for comparison with experimental data of Tewfik and Giedt[9]

Case	M_∞	Re, $\times 10^3$	T_∞,°R	T_{body},°R	T_b/T_∞	Purpose
I	5.73	2.05	71.4	Adiabatic	—	Determine C_p
II	5.73	2.05	71.4	378	5.3	Heat transfer
III	5.97	3.475	66.4	Adiabatic	—	Recovery factor

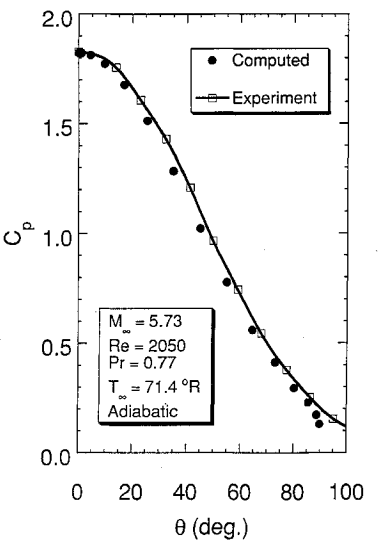

Fig. 4 Comparison of computed pressure coefficient along cylinder surface for case I of Table 2 with experimental data of Ref. 9.

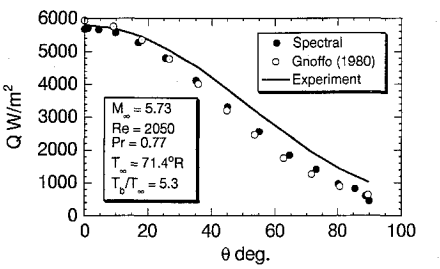

Fig. 5 Computed heat transfer along cylinder surface for case II of Table 2 compared with the experimental data of Ref. 9 and finite difference calculation of Ref. 10.

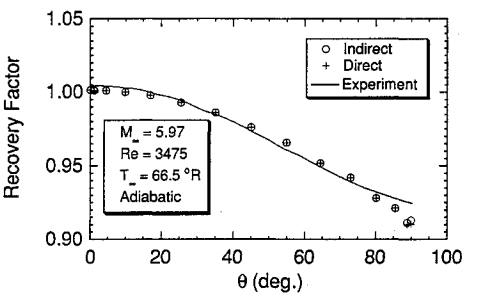

Fig. 6 Computed recovery factor for case III of Table 2 compared with the experimental data of Ref. 9.

temperature for cases I and II. Convergence of the maximum density residual to machine zero in 64 bits is shown in Fig. 3 for cases I and II on a 15×10 grid. The adiabatic surface condition used both the direct density calculation of Eq. (19) and the indirect one of Eq. (20). The convergence rate is virtually identical for the two adiabatic conditions, but both converge slightly slower than the isothermal case.

Figures 4–6 compare computed body surface quantities to the experimental data. Figure 4 compares the pressure along the surface of the cylinder for case I. The pressure coefficient

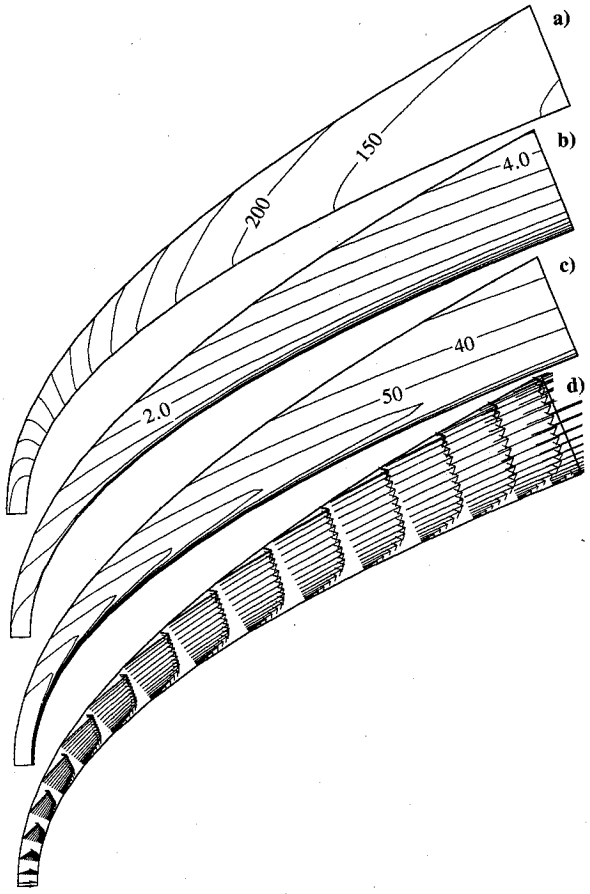

Fig. 7 Computed solution of the Mach 25 flow over an isothermal 5-deg hyperbolic cone. Shown are contours of the a) pressure, b) Mach number, c) temperature, and d) velocity vectors. The grid is shown in Fig. 1.

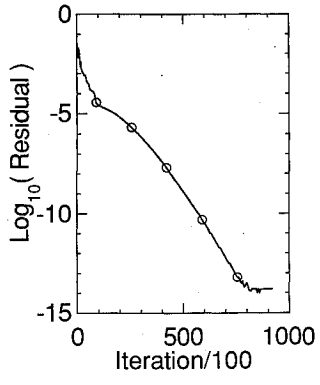

Fig. 8 Convergence of the density for the solution in Fig. 7.

$C_p = (p - p_\infty)/(\frac{1}{2}\gamma p_\infty M_\infty^2)$ is accurate to better then 10% except near $\theta = 90$ deg where the inviscid pressure was used as the outflow boundary condition. The value at the stagnation point differs by only 0.3%. Some numerical experiments were done where the outflow pressure was raised to match more closely the experimental pressure. This did not affect significantly the solution away from the outflow point.

Figure 5 compares the heat transfer profile of the isothermal case II to the experimental results and to a finite difference calculation of Gnoffo.[10] Plotted on this graph is the dimensional heat flux

$$Q^* = -\kappa^* \frac{\partial T^*}{\partial N^*} = -\left(\frac{\kappa_\infty T_\infty}{R}\right) \kappa \frac{\partial T}{\partial N} \qquad (26)$$

measured in W/m^2. The dimensional factor $\kappa_\infty = 3.4 \times 10^{-3}$ W/mK was computed from the Sutherland law and the data tabulated in Ref. 20. The shape of the heat transfer profile at the wall is consistent with both the finite difference and experimental results. At the stagnation point, the computed value differs from the experimental value by 2%. Away from the nose region, both the spectral and finite difference solutions underpredict the observed values.

Finally, Fig. 6 compares the computed body temperature of case III, represented as the recovery factor, with the experimental results,

$$\text{recovery factor} = \frac{T_{\text{body}} - T_\infty}{T_{\text{tot}_\infty} - T_\infty}$$

Table 3 Parameters for the flow over a 5-deg hyperbolic cone

M_∞	25
Re, $\times 10^4$	1.3034
Pr	0.72
T_∞, °R	486
T_{body}/T_∞	25

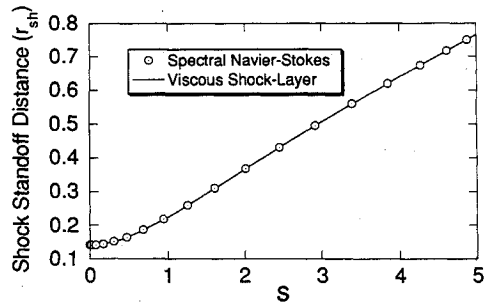

Fig. 9 Shock position as a function of arc length along the surface for the problem of Fig. 7.

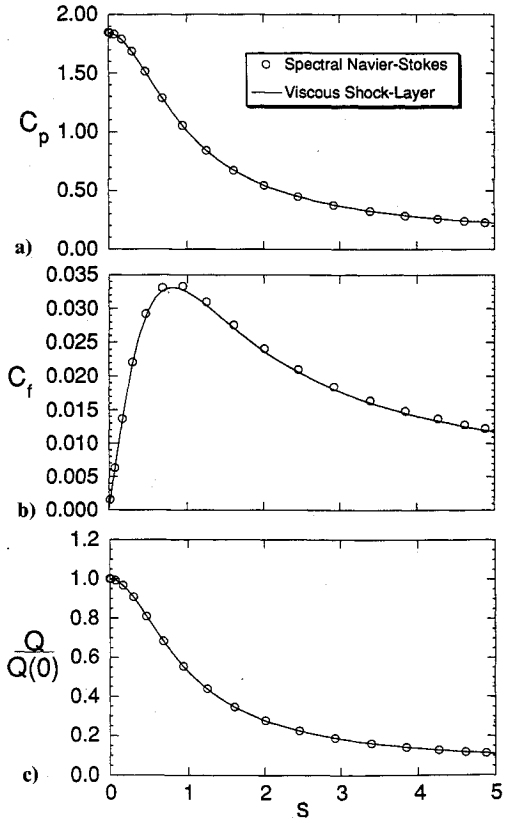

Fig. 10 Body surface quantities for the flow of Fig. 7: a) pressure coefficient; b) skin friction; and c) heat flux, normalized to the stagnation point value.

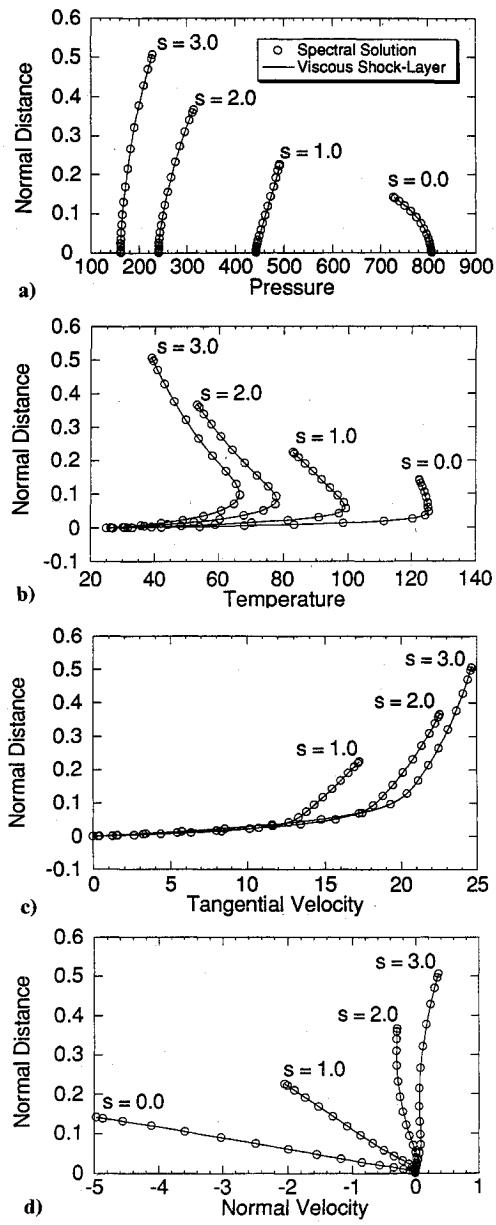

Fig. 11 Variation of flow quantities normal to the hyperbolic cone at four stations along the body: a) pressure, b) temperature, c) tangential velocity, and d) normal velocity.

Results for boundary treatments (19) and (20) are presented. Except near the outflow, the temperatures computed by the two methods differ by less than 0.01%. When compared with the experimental results, the computed temperatures are accurate to 0.5% for θ less than about 70 deg, after which the effects of the fixed exit boundary pressure can be seen.

Flow over a Hyperbolic Cone

To get a more detailed comparison, results of an $M = 25$ flow over a hyperbolic cone are compared with those of the shock-fitted finite difference VSL code of Ref. 18. Contours of the spectral solution are shown in Fig. 7. Convergence of the solution to steady state is shown in Fig. 8. Physical parameters for the calculation are shown in Table 3. For this problem, the shock thickness is estimated to be about 2×10^{-4}. We present results for the spectral code that used a 20×20 grid and $\sigma = 1.0$. With this grid, there were approximately 10 points maximum to resolve the boundary and thermal layers. At the shock, the minimum grid spacing is 2×10^{-3}, which is too large to resolve the shock. We remark that the 20×20 point spectral grid gave results that were virtually identical to the results of a 15×15 point grid except near the stagnation point where the temperature gradient is the largest. The finite difference calculation used 50 points in each direction. Thus, the spectral method has used only 16% of the total number of grid points that were used by the finite difference method.

We will compare the shock position and the wall quantities C_p, Q/Q_0, and C_f in the direction along the cone. We will also compare the profiles of the flow quantities in the direction normal to the cone surface at four stations along the length of the cone. We begin by comparing the shock position, shown in Fig. 9. Plotted is the normal distance of the shock from the body as a function of arc length along the body. At the nose, where the difference between the solutions can be exactly calculated, the standoff distance differs by only 4%.

Figure 10 compares the pressure coefficient, the heat flux, and the skin friction,

$$C_f = \frac{\mu}{\frac{1}{2}\gamma M_\infty^2} \frac{\partial q_\parallel}{\partial N}$$

along the body as a function of the distance from the nose. The worst agreement is seen in the comparison of the skin friction where the largest relative difference in C_f is 2.4%.

Variations of the pressure, temperature, and velocity in the direction normal to the body surface are compared at four stations along the body in Fig. 11. In all cases, we see excellent agreement between the spectral solution and the VSL solution. The temperatures, for instance, differ by less than 1% and the pressures by less than 2%. The worst comparison is between the normal velocities where the effects of the VSL approximation should be most significant. The normal velocity solutions differ by as much as 11% in the boundary layer where the normal velocity is small.

Conclusions

A Chebyshev spectral method has been designed to solve the viscous flow over a blunt body in a supersonic freestream. The shock is fitted as a sharp discontinuity. The boundary conditions at the body and at the outflow in the boundary layer use compatibility conditions similar to those used for inviscid flow calculations but include the viscous terms. When the body is adiabatic, the density at the body can be computed by a spectral extrapolation procedure or a compatibility equation. With these conditions, the method is stable and converges to a smooth steady-state solution without the need for artificial viscosity or filtering.

Solutions were computed over a circular cylinder in the Mach number range of 5.5–6.0 and over a hyperbolic cone at Mach 25. Reynolds numbers ranged from 2×10^3 to 1.3×10^4. The cylinder results were compared with experimental data and, with only about eight points in the boundary layer, were accurate to the 10% level. The computed results for the hyperboloid were compared with the results of a viscous shock-layer code. The calculations were performed with a maximum of 10 points in the boundary layer. Detailed comparisons of the normal profiles of all but the normal velocity showed agreement to within 1–2% with only about 16% the total number of grid points.

We have demonstrated the application of the Chebyshev spectral method only for the nose region and for relatively low Reynolds numbers. For higher Reynolds numbers and for longer bodies we expect it to be necessary to use a multidomain approach.[2,3] In that way, uniform resolution of the boundary layer would be possible by placing narrow subdomains near the body surface. The resolution requirements of longer bodies would be satisfied by using multiple subdomains in the streamwise direction.

Acknowledgments

This research was supported in part by NASA under Contract NAG1-862 and by the U.S. Department of Energy under Contract DE-FC05-85ER250000. The author would like to

thank Ajay Kumar for his viscous shock-layer results and Susan Ying for helpful comments.

References

[1]Kopriva, D. A., Zang, T. A., and Hussaini, M. Y., "Spectral Methods for the Euler Equations: The Blunt Body Problem Revisited," *AIAA Journal,* Vol. 9, No. 9, 1991, pp. 1458–1462.

[2]Kopriva, D. A., "Spectral Solution of Inviscid Supersonic Flows over Wedges and Axisymmetric Cones," *Computers and Fluids,* Vol. 21, No. 2, 1992, pp. 247–266.

[3]Kopriva, D. A., "Spectral Solutions of High-Speed Flows over Blunt Cones," AIAA Paper 92-0234, Jan. 1992; also, *AIAA Journal* (accepted for publication).

[4]Canuto, C., Hussaini, M. Y., Quarteroni, A., and Zang, T. A., *Spectral Methods in Fluid Mechanics,* Springer-Verlag, New York, 1987.

[5]Streett, C. L., Zang, T. A., and Hussaini, M. Y., "Spectral Methods for Solution of the Boundary-Layer Equations," AIAA Paper 84-1070, Jan. 1984.

[6]Pruett, C. D., and Streett, C. L., "A Spectral Collocation Method for Compressible, Non-Similar Boundary Layers," *International Journal on Numerical Methods in Fluids,* Vol. 13, No. 6, 1991, pp. 713–737.

[7]Yasuhara, M., Nakamura, Y., and Wang, J.-P., "Numerical Calculation of Hypersonic Flow by the Spectral Method," *11th International Conference on Numerical Methods in Fluid Dynamics,* edited by D. L. Dwoyer, M. Y. Hussaini, and R. G. Voigt, Vol. 323, Lecture Notes in Physics, Springer-Verlag, Berlin, Germany, 1989, pp. 607–611.

[8]Moretti, G., and Salas, M. D., "The Blunt Body Problem for a Viscous Rarefied Gas Flow," AIAA Paper 69-139, Jan. 1969.

[9]Tewfik, O. K., and Giedt, W. H., "Heat Transfer, Recovery Factor, and Pressure Distributions Around a Circular Cylinder Normal to a Supersonic Rarefied-Air Stream," *Journal of the Aerospace Sciences,* Vol. 27, No. 10, 1960, pp. 721–729.

[10]Gnoffo, P. A., "Complete Supersonic Flowfields over Blunt Bodies in a Generalized Orthogonal Coordinate System," *AIAA Journal,* Vol. 18, No. 6, 1980, pp. 611, 612.

[11]White, F. M., *Viscous Fluid Flow,* McGraw-Hill, New York, 1974.

[12]Canuto, C., "Boundary Conditions in Legendre and Chebyshev Methods," *SIAM Journal on Numerical Analysis,* Vol. 23, No. 2, 1986, pp. 815–831.

[13]Funaro, D., *Polynomial Approximation of Differential Equations,* Springer-Verlag, Berlin, Germany, 1992.

[14]Poinsot, T. J., and Lele, S. K., "Boundary Conditions for Direct Simulations of Compressible Viscous Reacting Flows," *Journal of Computational Physics,* Vol. 101, No. 1, 1992, pp. 104–129.

[15]Gustafsson, B., and Sundström, A., "Incompletely Parabolic Problems in Fluid Dynamics," *SIAM Journal on Applied Mathematics,* Vol. 35, No. 2, 1978, pp. 343–357.

[16]Oliger, J., and Sundström, A., "Theoretical and Practical Aspects of Some Initial Boundary Value Problems in Fluid Dynamics," *SIAM Journal on Applied Mathematics,* Vol. 35, No. 3, 1978, pp. 419–446.

[17]Dutt, P., "Stable Boundary Conditions and Difference Schemes for Navier-Stokes Equations," *SIAM Journal on Numerical Analysis,* Vol. 25, No. 2, 1988, pp. 245–267.

[18]Kumar, A., and Graves, R. A., "Numerical Solution of the Viscous Hypersonic Flow Past Blunted Cones at Angle of Attack," AIAA Paper 77-172, Jan. 1977.

[19]Kumar, A., private communication, 1991.

[20]Hilsenrath, J., Beckett, C. W., Benedict, W. S., Fano, L., Hoge, H., Masi, J., Nuttall, R., and Yeram, S. T., *Tables of Thermodynamic and Transport Properties,* Pergamon, New York, 1960.